EUROPEAN ORGANIZATION FOR NUCLEAR RESEARCH

CERN – PS DIVISION

CERN-PS-99-059 (DI)

CLOSED-ORBIT PROGNOSIS, CORRECTION AND MANIPULATION FOR THE PIMMS SYNCHROTRON

L. Badano[*)]

Closed-orbit control is a basic ingredient for the efficient performance of any circular accelerator. The paper summarises the results of the simulations of the expected orbit distortions before and after correction for the PIMMS (Proton Ion Medical Machine Study) synchrotron. Different situations that lead to a deterioration of the orbit, such as broken position monitors and correctors, misalignment of the magnetic and diagnostic elements with time, have been examined. In particular, the consequences of lowering the injection energy of the space-charge-dominated proton beam have been investigated. The possibility of local orbit correction during extraction by applying closed bumps has been analysed. Finally, on the basis of the demands of both the global orbit correction and the local corrections at top energy, the corrector dipoles specifications have been evaluated.

[*)] TERA Foundation and CERN

Also available on WWW, http://preprints.cern.ch

Geneva, Switzerland
17 December 1999

1. INTRODUCTION

This paper refers to the study of the expected orbit distortions before and after correction and of local orbit correction during extraction for the Proton-Ion Medical Machine Study (PIMMS) synchrotron. PIMMS is a collaboration between the Med-AUSTRON (Austria) and the TERA Foundation (Italy) hosted at CERN in the PS Division. The machine is designed for protons (injection energy 20 MeV, extraction energy from 60 to 250 MeV) and much higher rigidity fully stripped carbon ions (injection energy 7 MeV/u, extraction energy from 120 to 400 MeV/u).

Closed-orbit control is a basic ingredient for the efficient performance of any circular accelerator. Large closed-orbit distortions minimise the available aperture and affect the dynamics of the beam via non-linear elements. In PIMMS, for example, vertical closed-orbit errors in the resonance sextupole cause an increase of the horizontal emittance of the extracted beam. In an ideal accelerator, the closed orbit is defined as $y(s) = 0$, where y is a general co-ordinate that indicates the horizontal or vertical plane (x or z). In reality, the machine will inevitably contain many errors that will distort the orbit. The steel quality in the magnets and the packing factor of the laminations will not be entirely constant and the machining and alignment will not be perfect. All these errors will contribute to the closed-orbit distortion. Most will be random in nature, while others will be systematic and some may be time or field dependent. The particle motion in presence of dipolar field perturbations ΔB can be described by the equation [1]:

$$\frac{d^2}{ds^2} y + K(s)\, y = \mp \frac{\Delta B(s)}{B_0\, \rho_0} \tag{1}$$

where $K(s)$ is $(\rho_0^{-2} - k(s))$ for the horizontal motion and $k(s)$ for the vertical motion, B_0 is the bending field, ρ_0 the bending radius and $k(s)$ the quadrupole normalised gradient. The upper sign (-) refers to the horizontal plane and the lower sign (+) refers to the vertical plane. The solution of equation (1), which gives the closed-orbit distortion with respect to the ideal orbit is:

$$y(s) = \mp \frac{\beta_y^{\frac{1}{2}}(s)}{2 \sin \pi Q_y} \int_0^C \beta_y^{\frac{1}{2}}(\sigma)\, \frac{\Delta B(\sigma)}{B_0\, \rho_0} \cos\left(\left|\mu(\sigma) - \mu(s)\right| - \pi\, Q\right) d\sigma \tag{2}$$

where β is the betatron amplitude function and Q is the tune. For short field errors (i.e. β, μ, ΔB constant over the length ℓ of the field error), the integral in (2) can be replaced by a summation over the errors.

$$y(s) = \mp \frac{\beta_y^{\frac{1}{2}}(s)}{2 \sin \pi Q_y} \sum_n \beta_{yn}^{\frac{1}{2}}\, \delta_n \cos\left(\left|\mu_n - \mu(s)\right| - \pi\, Q\right) \qquad \text{where } \delta_n = \mp \frac{(\ell\, \Delta B)_n}{B_0\, \rho_0} \ . \tag{3}$$

Dipole field errors, ΔB, generate kicks given by:

$$\delta_y = \varphi \frac{\Delta B}{B} \quad \text{where } \varphi = \ell / \rho_0 \text{ is the bend angle of the element.} \tag{4}$$

Quadrupoles generate kick errors in the same plane as transverse shifts Δx, Δy:

$$\delta_x = k\, \ell_q\, \Delta x \quad \text{and} \quad \delta_z = k\, \ell_q\, \Delta z\,. \tag{5}$$

Longitudinally shifted dipoles generate opposed kicks at the entry and exit of the dipole,

$$\delta_{\text{upstream}} = -\rho_0^{-1}\, \Delta s \quad \text{and} \quad \delta_{\text{downstream}} = \rho_0^{-1}\, \Delta s\,. \tag{6}$$

Finally, dipoles tilted about the longitudinal axis by $\Delta\theta$ generate kicks in the orthogonal plane:

$$\delta = \varphi\, \Delta\theta\,. \tag{7}$$

This paper summarises:

- Closed-orbit requirements and tolerances for the PIMMS (Proton Ion Medical Machine Study) synchrotron.
- Simulations of the expected distortion and corrected orbits for non-space charge conditions. This corresponds to carbon ion operation at all energies and protons at high energies. In particular calculations are made on the extraction working point since this influences the quality of the extracted beam.
- Simulations of the expected distortion and corrected orbits for space-charge conditions. This corresponds to the protons at injection and influences the choice of the injection energy.
- Sensitivity to missing position monitors and correctors.
- Degradation of the closed orbit with time and a prognosis for the frequency of realignment.
- Local orbit correction with 3-, 4- and 5-magnet bumps.
- Specifications of the correction dipoles.

The results reported in this paper have been obtained using two accelerator codes, AGILE [2] and MAD [3]. Both codes base the correction process on a least squares minimisation that diminishes the deviation from an ideal orbit at the position monitors [4]. A series of test runs showed that the results obtained from the two programs did not differ by more than a few per cent. It was therefore decided to use one code or the other according to its efficiency in solving a specific problem. In each section, the choice of program is indicated. Some of the simulations were performed with a sample of 1000 randomly generated machines, others with only 200 or 100 machines. This depends on the program used (the AGILE running time is longer than MAD in many cases) and the precision required to solve a specific problem.

2. CLOSED-ORBIT PROGNOSIS AND CORRECTION

2.1 Requirements for closed-orbit correction and control

The basic guidelines for the closed-orbit correction and control for PIMMS are:

- For injection and acceleration, the global closed orbit must be within ± 10 mm horizontally and ± 7.5 mm vertically.
- For extraction, the global closed-orbit correction must be within ± 5 mm in both planes. This provides space for local corrections, see last point.
- For extraction, local corrections are needed at the septa and sextupoles to be better than ± 1 mm.
- When adding a local correction, the closed orbit may degrade elsewhere, but must never exceed the global limits of ± 10 mm horizontally and ± 7.5 mm vertically.

2.2 Alignment and field tolerances

The errors responsible for orbit distortion considered for PIMMS are listed in Table 1.

Tolerances for magnetic elements and position monitors	
Assumed alignment tolerances	**Tolerance**
Alignment tolerances: Δx_{RMS}, Δz_{RMS}, Δs_{RMS} [m]	0.3×10^{-3}
Tilt about all three co-ordinate axes, $\Delta\theta_{RMS}$ [rad]	0.3×10^{-3}
Cut-off for alignment and tilt errors	$3\,\sigma$
Assumed position monitor reading errors	
Uniform distribution [mm]	± 0.1
Estimated magnet manufacturing tolerances	
Integrated relative dipole field error at low field, $(\Delta BL/BL)_{RMS}$	1.2×10^{-3}
Integrated relative. dipole field error at high field $(\Delta BL/BL)_{RMS}$	1.2×10^{-3}
Integrated relative corrector field error, $(\Delta BL/BL)_{RMS}$	1.0×10^{-2}
Cut off for all field errors	$3\,\sigma$

Table 1 *Tolerances for magnet elements and position monitors.*

It is assumed that the ring is aligned with equipment and techniques that are standard and not pushed to the limit of their performance. The tolerances to be expected from a standard alignment were established with CERN expert help [5]. The main dipole field error (1.2×10^{-3}) is obtained by combining quadratically, at low field, the dominant remanent field error (8.4×10^{-4}) with the length error (8.0×10^{-4}) or, at high field, the dominant packing factor field error (8.4×10^{-4}) with the length error (8.0×10^{-4}) [6]. This is based on the packing factor tolerance being adjusted so that its field error is equal to the remanent field error for the proton beam injection at 20 MeV. Correctors and position monitors are also considered to be affected by errors. The correctors, being weaker than the main dipoles, are allowed a larger relative field error [6]. The position monitors have both alignment and reading errors. Alignment and field errors are applied to all elements according to a gaussian distribution cut at 3 standard deviations, while monitor reading errors are given a uniform distribution.

2.3 Sensitivity to Errors

In order to determine the relative importance of the different errors, a series of runs were made with samples of 200 machines. The orbits have been calculated with the program MAD on the extraction working point (Q_x = 1.667, Q_z = 1.720). The absolute maximum excursions are always quoted (here and in the rest of the paper), since these values are of more direct interest for the aperture than the peak-to-peak values. An analysis of the data is summarised in Table 2.

Sensitivity to the different errors

	Average maximum excursions of the orbits:	
Error source	**Horizontal**	**Vertical**
Relative dipole field error (1.2×10^{-3})	12.5 mm	-
Transverse quadrupole shifts (0.3×10^{-3} m)	1.5 mm	1.9 mm
Longitudinal dipole shift (0.3×10^{-3} m)	0.6 mm	-
Tilt of dipoles (0.3×10^{-3} rad)	-	4 mm

Table 2 *Sensitivity to the different field errors.*

It is evident from Table 2 that the horizontal orbit is most strongly affected, in decreasing order of magnitude, by field errors of the main dipoles, by horizontal quadrupole shifts and by longitudinal main dipole shifts. The vertical orbit is mainly affected by tilts about the longitudinal axis of the main dipoles and by vertical shifts of the quadrupoles.

2.4 Monitoring and correction systems

The layout of the PIMMS lattice together with the monitoring and correction systems is shown in Figure 1. The reasons for placing the position monitors and correction dipoles in pairs at the local maxima of the betatron amplitude functions are given in Reference 6. Figure 2 shows the horizontal monitors and horizontal correctors distribution with the horizontal phase advance versus distance. Figure 3 shows the vertical monitors and vertical correctors distribution with the vertical phase advance versus distance.

It is evident from the two figures that the distribution of position monitors and correctors with phase advance is more regular in the vertical plane and that the vertical monitors have the advantage of being exactly at the maxima of the betatron amplitude function. As the number and regularity of the monitors per phase advance define the sampling of closed orbit, the vertical correction scheme will be the more efficient (see Section 2.8). The precision and reliability of the measurement system [7] are extremely important, as they determine the quality of the correction together with the precision of the correctors and their maximum strength (see Section 4).

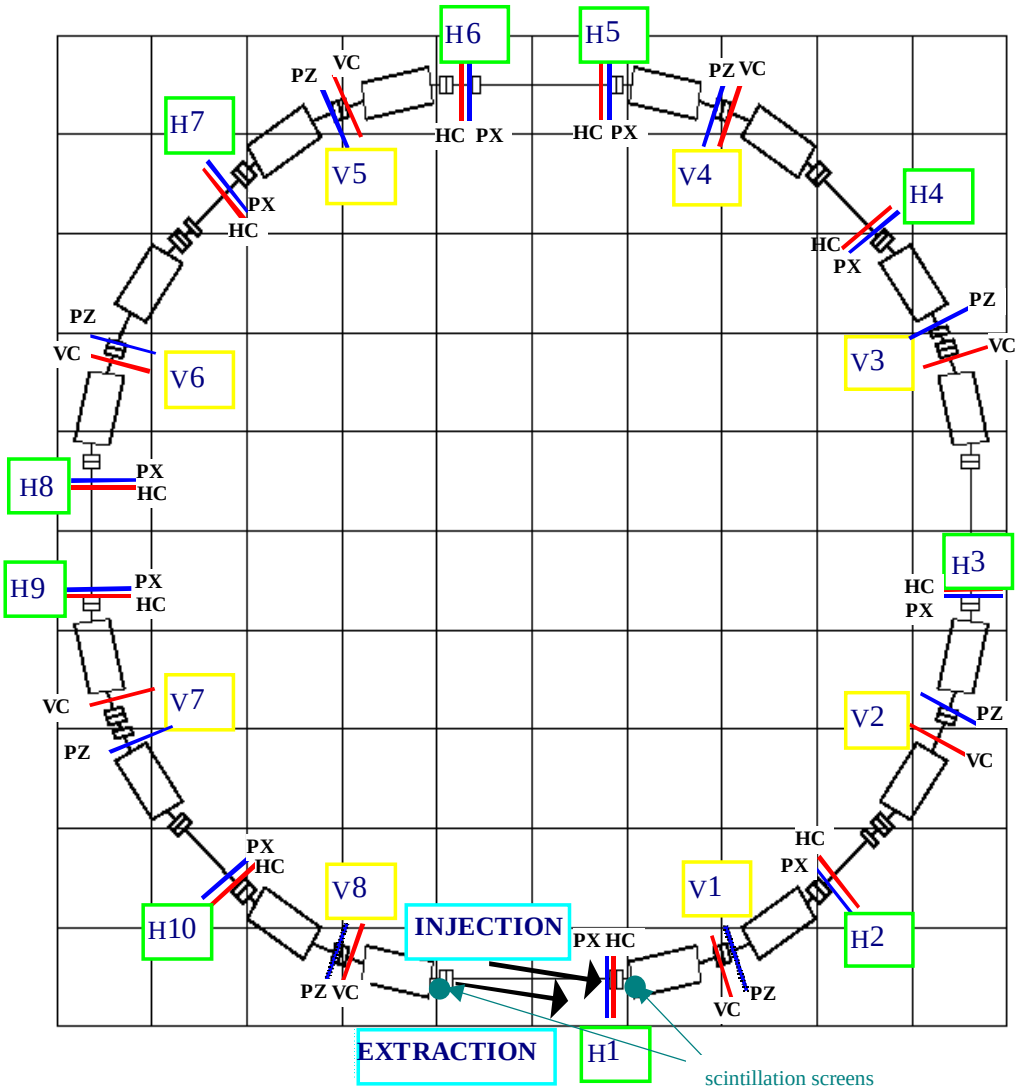

Figure 1. *Layout of the PIMMS lattice with beam position monitoring and correction systems. (H1,…10: horizontal measurement/correction stations with PX monitors and HC correctors; V1,…8: vertical measurement/correction stations with PZ monitors and VC correctors.*

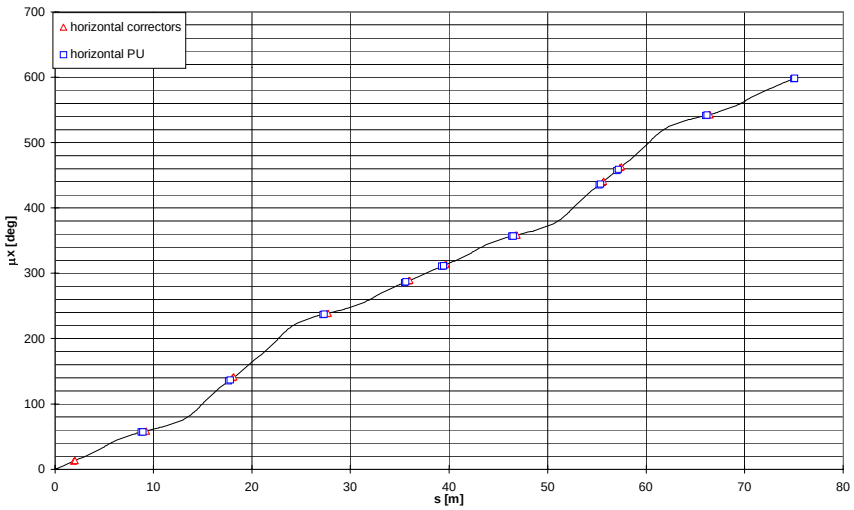

Figure 2 *Horizontal position monitors and correctors distribution with the horizontal phase advance versus distance (the triangles represents the horizontal correctors, while the squares represents the horizontal position monitors).*

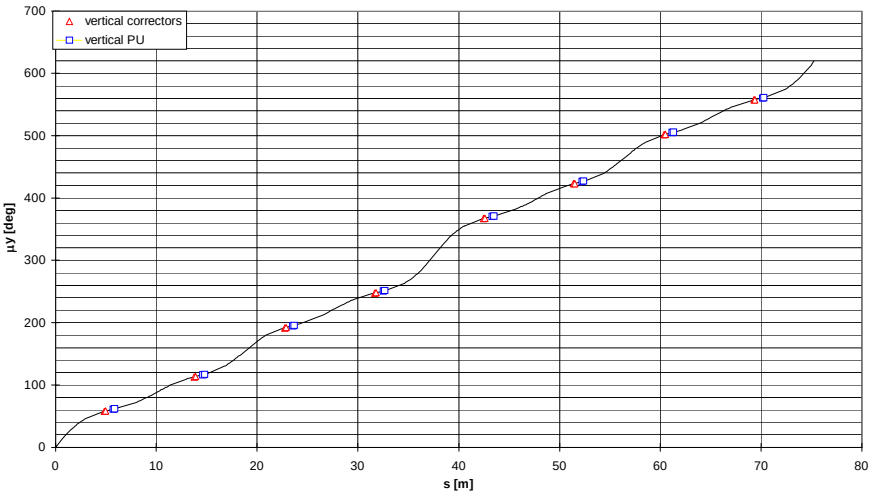

Figure 3 *Vertical position monitors and correctors distribution with the vertical phase advance versus distance (the triangles represents the vertical correctors, while the squares represents the vertical position monitors).*

2.5 Closed-orbit prognosis and correction for non-space-charge conditions

Non-space-charge conditions exist for all beams except the injection of protons. One thousand machines with random errors have been analysed before and after correction on the extraction working point ($Q_x = 1.667$, $Q_z = 1.720$). The basic data, obtained with MAD, are presented in Figures 4 (a) and (b) for the horizontal plane and Figures 5 (a) and (b) for the vertical plane. The expected distributions of the strengths of the horizontal and vertical correctors are shown in Figures 6 and 7 respectively. An analysis of these data is summarised in Table 3. With 'normalised standard deviation' is meant the standard deviation of the distribution divided by the average value.

Prognosis for closed orbits at extraction and their correction

	Before correction		**After correction**	
	Horizontal	**Vertical**	**Horizontal**	**Vertical**
Average of max. excursions μ [mm]	11.9	4.3	1.6	0.6
Max. absolute excursion [mm]	37.7	13.4	3.5	1.2
Normalised standard deviation σ/μ	0.42	0.40	0.31	0.25
Average of max. kicks [mrad]	-	-	0.94	0.28
Max. corrector kick [mrad]	-	-	2.09	0.65
Closed-orbit tolerance [mm]	±10	±7.5	±5	±5
% of machines within tolerance	41	96	100	100

Table 3 *Prognosis for closed orbits at extraction and their correction.*

Table 3 shows that the expected situation is quite comfortable for extraction. With standard alignment techniques, 41% of the machines before correction in the horizontal plane and 96% in the vertical plane would be within the allowed global closed-orbit margin. After correction, all machines would be well within the stricter tolerances for extraction. The normalised standard deviations show that the

distribution of the maximum absolute orbit excursion changes before and after correction.

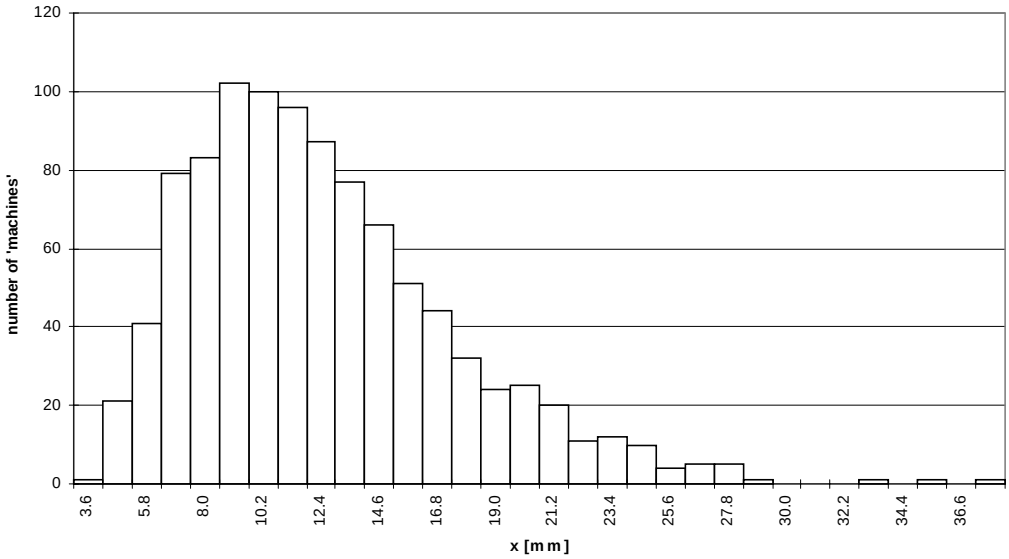

(a) Horizontal, maximum absolute excursions of the closed orbit before correction

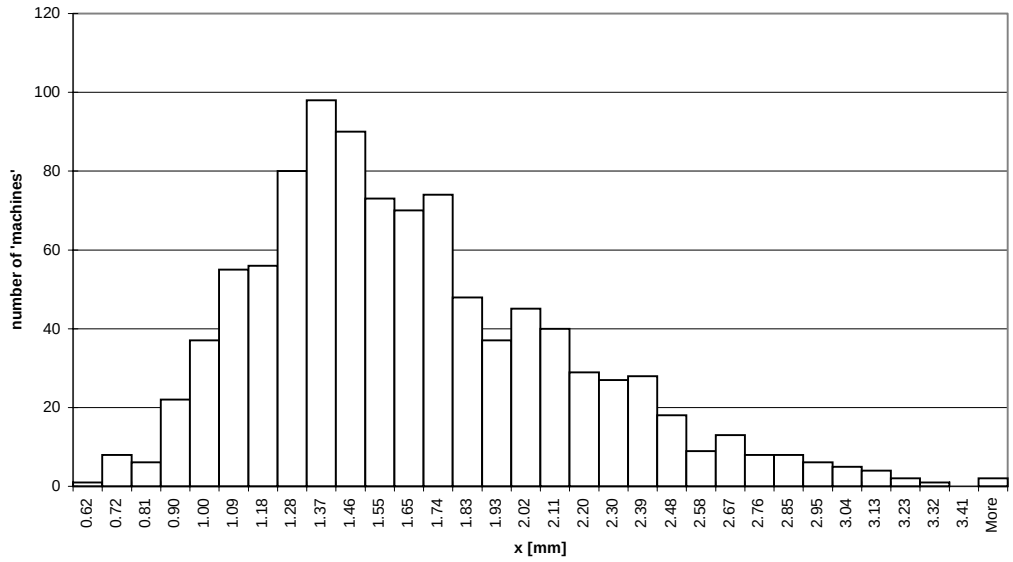

(b) Horizontal, maximum absolute excursions of the closed orbit after correction

Figure 4 *Statistics for 1000 randomly generated, horizontal, closed orbits before and after correction at extraction [Q_x = 1.667, Q_z = 1.720, all correctors and monitors working] - Note the change of scale.*

Although Figures 4 and 5 and Table 3 are based on the use of all position monitors and correctors, it should be noted that a correction typically requires a reduced number of units to reach a satisfactory level (providing the correctors are the most efficient for the chosen orbit), after which any additional correctors become less efficient and, in practice, may even lead to a slight degradation of the correction.

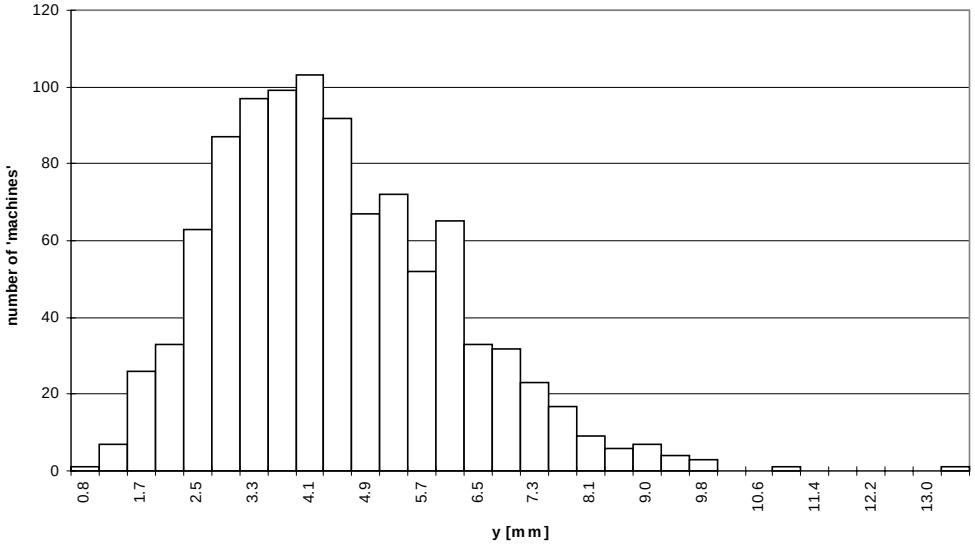

(a) Vertical, maximum absolute excursions of the closed orbit before correction

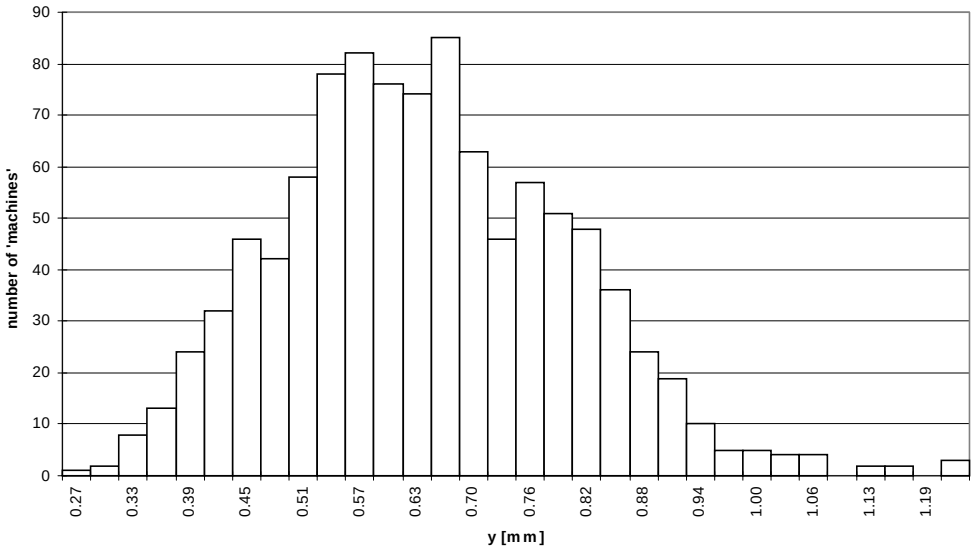

(b) Vertical, maximum absolute excursions of the closed orbit after correction

Figure 5 *Statistics for 1000 randomly generated, vertical, closed orbits before and after correction at extraction [Q_x = 1.667, Q_z = 1.720, all correctors and monitors working] - Note the change of scale.*

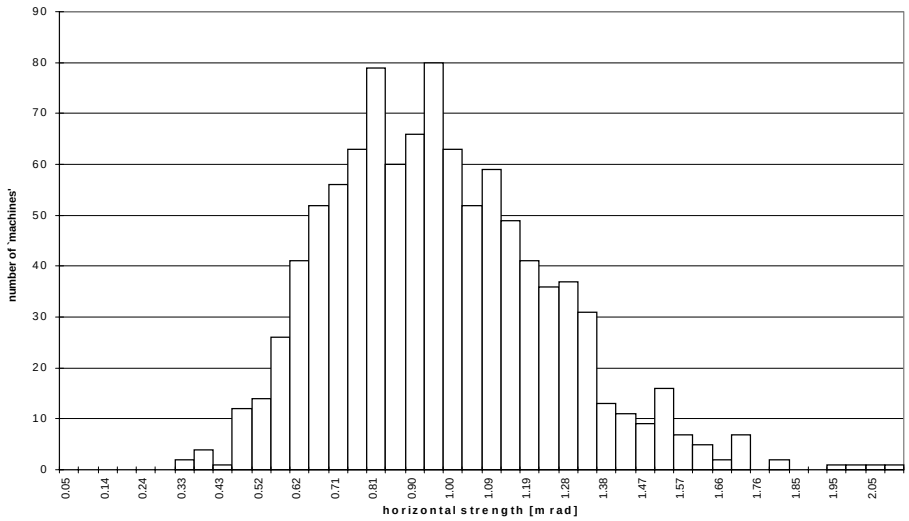

Figure 6 *Expected distribution of the maximum absolute horizontal corrector strength [Q_x = 1.667, Q_z = 1.720, all correctors and monitors working].*

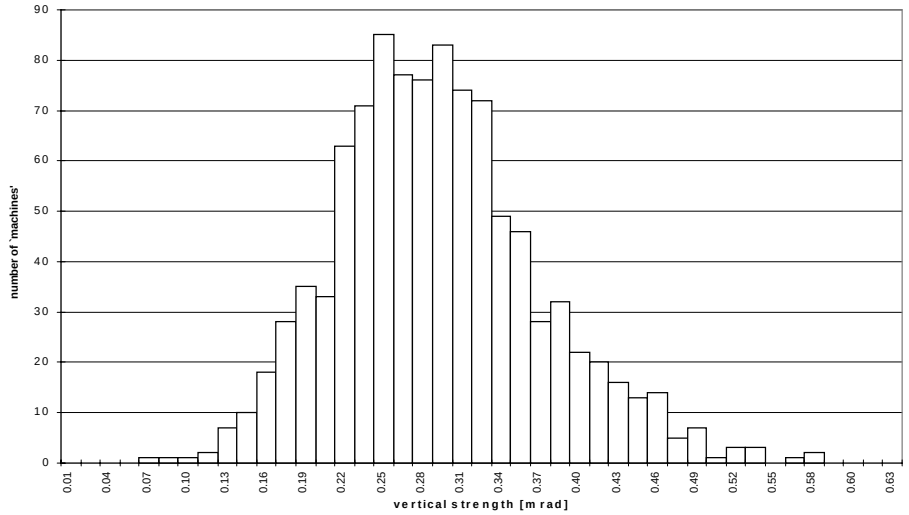

Figure 7 *Expected distribution of the maximum absolute vertical corrector strength [Q_x = 1.667, Q_z = 1.720, all correctors and monitors working].*

2.6 Closed-orbit prognosis and correction for injection with space charge

This section considers two additional factors that cause a deterioration of the closed orbit with respect to the relatively comfortable conditions described in the previous section. These factors apply only to the proton beam:

- The effect of space charge that dominates the injection of the high-intensity proton beam (6×10^{10} protons).
- The possible lowering of the injection energy of the protons.

Space charge affects the closed orbit indirectly via incoherent tune shifts. Before injection, the unloaded working point is displaced upwards in the tune diagram, so that once the full space charge load is added, the beam will occupy the nominal storage region (Q_x = 1.680, Q_z = 1.720). The unloaded working point is much closer to the integer resonance and, as a result, the oscillations of the betatron amplitude functions (and hence the beam size and orbit distortions) are increased. Since synchrotron oscillations cycle the particles through the full length of the bunch, the

particles see the full range tune values corresponding to quasi-zero space charge at the extremities of the bunch to maximum at the middle. The unloaded working point that has the largest orbit distortions is therefore used for aperture calculations.

The 7 MeV/u carbon-ion beam has approximately the same rigidity as the 28 MeV proton beam. However 20 MeV protons have been chosen for reasons of availability of a commercial linear accelerator. Although the nominal injection energy of the protons is 20 MeV, 11 MeV and 7 MeV have also been considered in the following simulations for reasons of cost savings. The last value is of particular interest, since it would fit with using the same linac for both the proton and carbon ion beams [8, 9].

The orbits have been calculated on the de-tuned working points:

- $Q_x = 1.754$, $Q_z = 1.815$ at 20 MeV,
- $Q_x = 1.796$, $Q_z = 1.882$ at 11 MeV,
- $Q_x = 1.820$, $Q_z = 1.911$ at 7 MeV.

The relative field error considered at 20 MeV is quoted in Table 1. At 11 MeV and 7 MeV, the relative error from the remanent field increases and the overall errors become 1.4×10^{-3} and 1.5×10^{-3} respectively. One thousand machines with random errors have been analysed before and after correction at the three injection energies with MAD. The basic data at 20 MeV are presented in Figures 8 (a) and (b) for the horizontal plane and Figures 9 (a) and (b) for the vertical. An analysis of this data is summarised in Table 4. The corresponding analysis of the 11 MeV and 7 MeV data is summarised in Tables 5 and 6 respectively.

The injection orbits of Tables 4, 5 and 6 have been calculated with the sextupoles switched off, as it is not possible to find closed orbits for all the 1000 machines with the sextupoles on at the lower injection energies 7 MeV and 11 MeV. This is required because large orbit excursions in the non-linear field of the sextupoles introduces kicks that make the machine unstable. In fact, this occurs in practice and at injection the sextupoles should therefore be switched off or switched on at a small fraction of their nominal strength. For injection at 20 MeV, the distorted orbits are smaller, the non-linearities are less important and the correction algorithm works with the sextupoles on or off with only minor variations in the maximum values of the distortion.

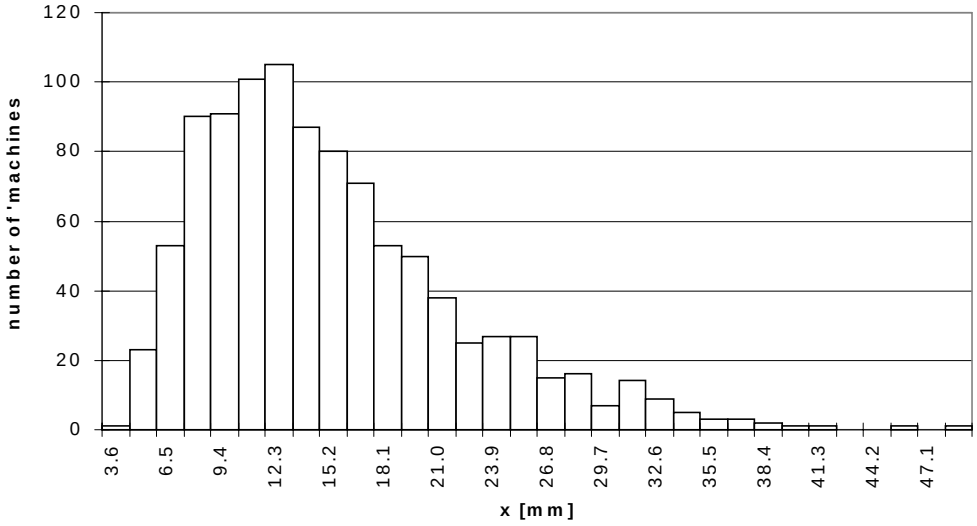

(a) Horizontal, maximum absolute excursions of the closed orbit before correction

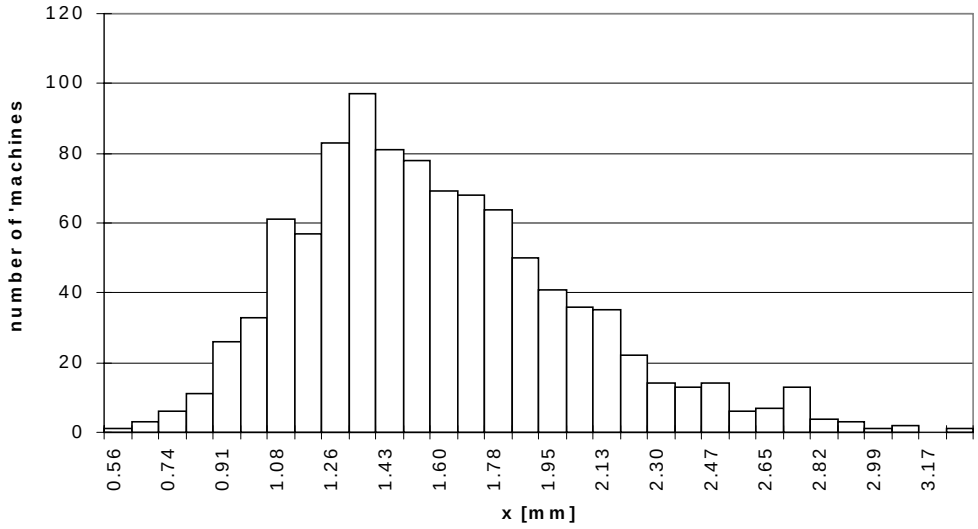

(b) Horizontal, maximum absolute excursions of the closed orbit after correction

Figure 8 *Statistics for 1000 randomly generated, horizontal, closed orbits before and after correction at injection (20 MeV) [Q_x = 1.754, Q_z = 1.815, all correctors and monitors working] - Note the change of scale.*

A comparison between Tables 4, 5 and 6 shows that the expected situation becomes more critical as the injection energy is lowered. In Table 4, the expected situation is rather comfortable for injection at 20 MeV. With standard alignment techniques, 30% of the machines in the horizontal plane and 70% in the vertical plane would be within the allowed closed-orbit margins and could be injected with full intensity without beam loss. Whereas, at 11 MeV, 16% of the machines in the horizontal plane and 40% in the vertical plane would be within the allowed closed-orbit margins and, at 7 MeV, only 12% of the machines in the horizontal plane and 24% in the vertical plane would be within the allowed closed-orbit margins. However after correction, all machines at all energies would, in any case, be within the closed-orbit tolerances for injection and also within the stricter tolerances for extraction. Figures 10 (a) and (b)

illustrate these results showing the percentage of orbits before correction that have their maximum excursion within the allowed closed-orbit margins versus injection energy. This is an indication of the difficulty that will be experienced establishing the first turn before a correction can be applied.

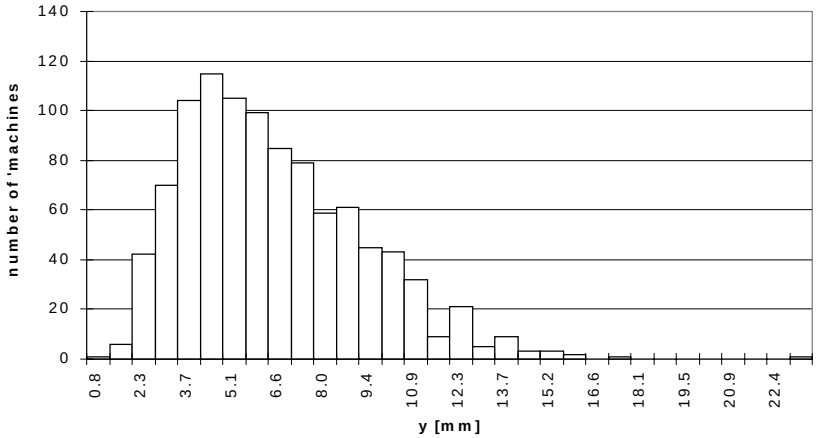

(a) Vertical, maximum absolute excursions of the closed orbit before correction

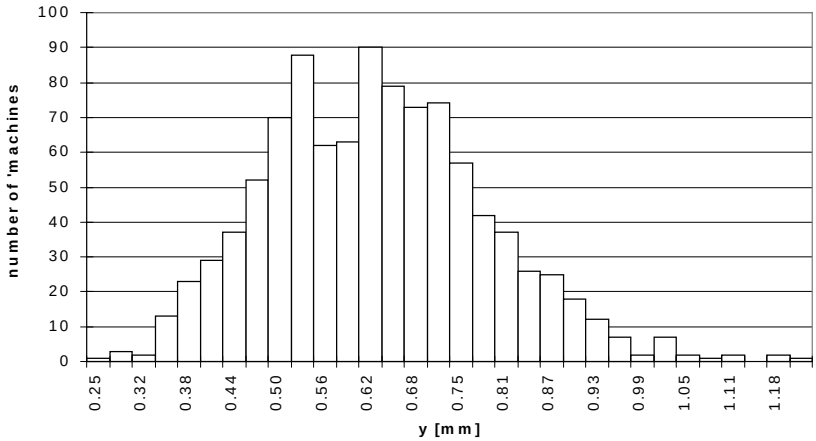

(b) Vertical, maximum absolute excursions of the closed orbit after correction

Figure 9 *Statistics for 1000 randomly generated, vertical, closed orbits before and after correction at injection (20 MeV) [Q_x = 1.754, Q_z = 1.815, all correctors and monitors working]. - Note the change of scale.*

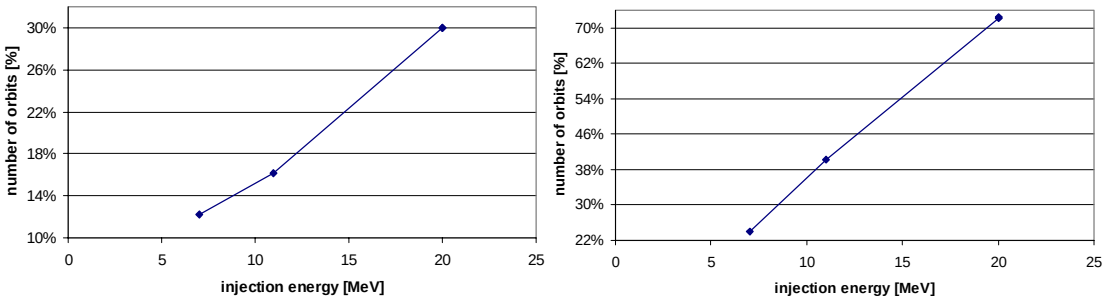

(a) Horizontal plane *(b) Vertical plane*

Figure 10 *Percentage of orbits before correction with the maximum excursion within the allowed closed-orbit injection margins versus energy.*

Prognosis for closed orbits at injection (20 MeV) and their correction				
	Before correction		**After correction**	
	Horizontal	**Vertical**	**Horizontal**	**Vertical**
Average of max. excursions μ [mm]	14.3	6.0	1.5	0.6
Max. absolute excursion [mm]	48.6	23.1	3.3	1.2
Normalised standard deviation σ/μ	0.48	0.47	0.29	0.24
Average of max. kicks [mrad]	-	-	0.94	0.29
Max. corrector kick [mrad]	-	-	2.09	0.66
Closed-orbit tolerance [mm]	±10	±7.5	±10	±7.5
% of machines within tolerance	30	72	100	100

Table 4 *Prognosis for closed orbits at nominal injection (20 MeV) and their correction [Q_x = 1.754, Q_z = 1.815].*

Prognosis for closed orbits at injection (11 MeV) and their correction				
	Before correction		**After correction**	
	Horizontal	**Vertical**	**Horizontal**	**Vertical**
Average of max. excursions μ [mm]	19.7	10.0	1.8	0.6
Max. absolute excursion [mm]	71.4	45.4	3.7	1.2
Normalised standard deviation σ/μ	0.53	0.57	0.29	0.25
Average of max. kicks [mrad]	-	-	1.09	0.29
Max. corrector kick [mrad]	-	-	2.30	0.67
Closed-orbit tolerance [mm]	±10	±7.5	±10	±7.5
% of machines within tolerance	16	40	100	100

Table 5 *Prognosis for closed orbits at intermediate injection energy (11 MeV) and their correction [Q_x = 1.796, Q_z = 1.882].*

Prognosis for closed orbits at injection (7 MeV) and their correction				
	Before correction		**After correction**	
	Horizontal	**Vertical**	**Horizontal**	**Vertical**
Average of max. excursions μ [mm]	22.6	15.1	1.8	0.7
Max. absolute excursion [mm]	84.9	74.2	3.8	2.0
Normalised standard deviation σ/μ	0.56	0.62	0.29	0.31
Average of max. kicks [mrad]	-	-	1.16	0.28
Max. corrector kick [mrad]	-	-	2.52	0.65
Closed-orbit tolerance [mm]	±10	±7.5	±10	±7.5
% of machines within tolerance	12	24	100	100

Table 6 *Prognosis for closed orbits at lower injection energy (7 MeV) and their correction [Q_x = 1.820, Q_z = 1.911].*

2.7 Available aperture versus injection energy

The vacuum chamber aperture for the PIMMS synchrotron has been decided as a function of the maximum beam size, the closed-orbit margin and a collimation margin that makes use of the 'poor'-field region [10]. In the vertical plane, the carbon ion beam at injection fixes the maximum beam size, whereas in the horizontal plane the maximum beam size is the space required by the separatrices of the slow extraction.

At injection, the 7 MeV/u carbon-ion beam fits tightly within the aperture whereas the 20 MeV proton beam is smaller and has space to spare. As the proton injection energy is lowered, the deterioration of the orbit together with the increase in emittance progressively reduces the excess aperture with respect to the carbon ion beam and eventually sets a limit to the minimum acceptable injection energy for protons. To see approximately where this aperture limits occurs, the maximum total horizontal and vertical half beam sizes of the protons have been plotted in Figures 11 (a) and (b) against injection energy. The injection beam sizes for the 7 MeV/u carbon ions are shown as dotted lines in the same figures for comparison. Once the proton beam exceeds the injected carbon-ion beam dimensions, the proton beam is too large to be able to respect the allowed margins.

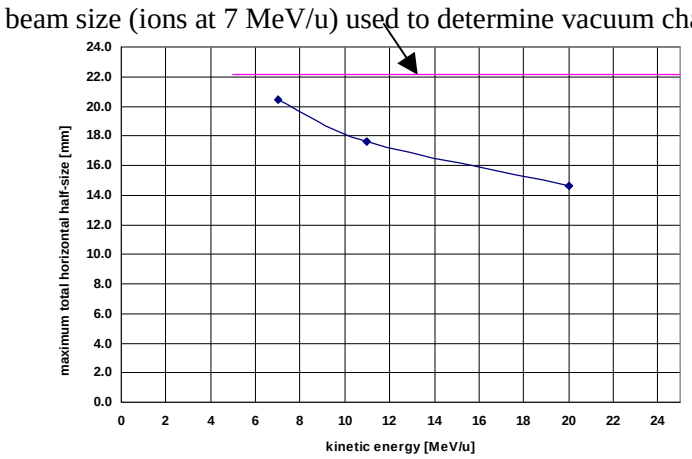

(a) Horizontal

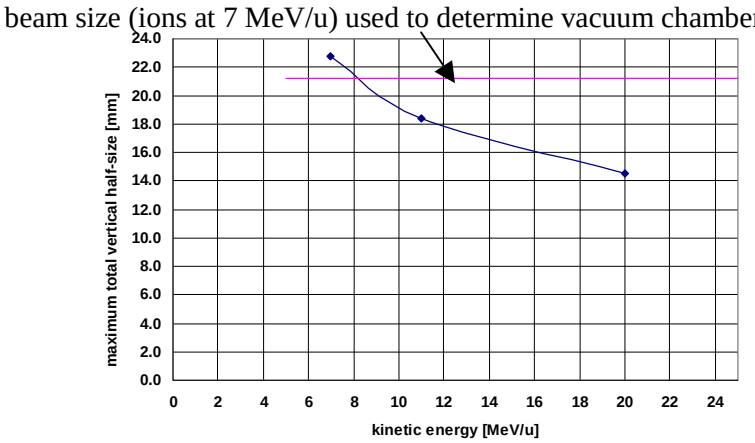

(b) Vertical

Figure 11 *Maximum total proton beam half-size versus injection energy.*

In the horizontal plane (Figure 10) the beam is still slightly smaller than the carbon ion beam and sits comfortably within the space originally determined by separatrices.

From Figure 11, an injection energy of 7 MeV appears to be an acceptable compromise in which the vertical condition is just exceeded.

2.8 Effect of missing position monitors and correctors

The aim of this section is to verify the quality of the position monitoring and correction systems shown in Figure 1 in terms of its sensitivity to missing elements. The sensitivity to missing monitors is investigated in the horizontal plane by taking random samples of 200 machines under space-charge conditions and correcting orbits for various patterns of missing monitors. In all the simulations performed with AGILE, there is an extra monitor in the injection-extraction straight section, just after the electrostatic septum, compared to the lay-out shown in Figure 1 used for the simulations with MAD. The quality of the correction is quantified by taking the ratio between the average of the absolute maximum excursions in the initial orbits and the average of the absolute maxima after correction (see Table 7).

Sensitivity to missing position monitors	
Randomly chosen samples of 200 machines	**Ratio of average of maximum excursions of orbits before and after correction**
ALL monitors (11) and all correctors (10)	10.5
One monitor missing*	9.5, 6.0, 10.1, 10.3, 3.8, 9.2, 4.6, 4.1, 3.7, 9.0
Two consecutive monitors missing*	5.0, 3.8, 3.6, 3.0, 3.1
Two non-consecutive monitors missing*	9.2, 3.6,3.9,3.7,3.4
Three consecutive monitors missing*	2.0, 2.7, 2.5
Three non-consecutive monitors missing*	4.3

* The number of correctors used was always one less than the number of monitors, but these were the most efficient correctors chosen from the full complement.

Table 7 *Sensitivity to missing monitors (Q_x = 1.754, Q_z = 1.815).*

The reference calculation in Table 7 shows that with a full complement of position monitors and correctors one can expect on average to reduce the beam excursions by a factor of 10.5. When removing a single monitor either the loss of efficiency is small with an improvement between 9 and 10, or much poorer with an improvement of only 3.7 to 6. This result correlates with the distance to neighbouring monitors. The three cases where pairs of monitors are close in betatron phase (see Figure 2) give the six high efficiencies and the intermediate monitors that are more isolated give the poorer results. When two consecutive monitors are missing, this nearly always results in a large gap in betatron phase and the efficiency drops directly, in all but one case, to between 3.4 and 3.9. With three consecutive monitors missing, there is, unsurprisingly, an even poorer improvement of only 2 to 2.7.

For the purpose of injection, two consecutive, missing monitors, or up to 3 non-consecutive monitors, would in the majority of the cases be acceptable. However, for extraction the orbit should be better corrected ($\pm$ 5 mm) and if one of the missing monitors should be needed for tuning the beam position in the septa or in the sextupoles, then the situation could be critical. Thus, with only a single missing

monitor, it will be a question of chance whether the extraction can be adjusted correctly.

The simulations described in the previous sections show that the correction dipoles in both planes are used more or less uniformly. The only significant exception is a pair of horizontal correctors in the rf drift space (stations H5 and H6 of Figure 1) that effectively share the load that would normally be applied to a single unit. Some tests made by selecting the best group of 2, 3, 4 etc. up to the maximum number of correctors did not show any significant change in the average corrector strength, only an improvement in the corrected orbit and an increase of the maximum kicks. Table 8 summarises the data analysis of the simulation (MAD) of 1000 machines with non-space-charge working conditions with the best 6 or 4 correctors per plane.

Prognosis for closed orbits at extraction with reduced number of correctors

	All	6/plane	4/plane
Horizontal plane uncorrected			
Average of absolute maximum excursions [mm]	11.9	11.9	11.9
Maximum absolute excursion [mm]	37.7	37.7	37.7
Horizontal plane corrected			
Average of absolute maximum excursions [mm]	1.6	1.9	2.8
Maximum absolute excursion [mm]	3.5	5.3	8.6
Average of maximum corrector kicks [mrad]	0.94	0.96	1.04
Maximum corrector kick [mrad]	2.09	2.22	2.75
Vertical plane uncorrected			
Average of absolute maximum excursions [mm]	4.3	4.3	4.3
Maximum absolute excursion [mm]	13.4	13.4	13.4
Vertical plane corrected			
Average of absolute maximum excursions [mm]	0.63	0.71	0.98
Maximum absolute excursion [mm]	1.22	1.65	3.04
Average of maximum corrector kicks [mrad]	0.28	0.29	0.30
Maximum corrector kick [mrad]	0.65	0.72	0.87

Table 8 *Prognosis for closed orbits at extraction with reduced number of correctors.*

The sensitivity of the machine to missing correctors is investigated with randomly-generated groups of 200 machines with non-space-charge working conditions and for various patterns of missing correctors (for the name of correctors and position monitors refer to Figure 1). It should be remembered that the orbit is less distorted without space charge compared to with space charge. The results are summarised in Table 9. In Table 9, the horizontal corrector HC31 (station H8 of Figure 1) is an example of a corrector with a nearby neighbour and corrector HC36 (station H10 of Figure 1) is a more typical case of a uniformly spaced corrector. Removing the former has little impact on the closed-orbit correction or the corrector strengths, whereas removing the latter approximately doubles the amplitude of the corrected closed orbit and the corrector strengths. As will be seen in Section 4, the corrector strengths will not be able to satisfy such large increases even if the orbit is still good enough. Removing both of these correctors, leads to a stronger deterioration of the orbit to the point where the tail of the distribution after correction is outside the tolerance. The poorer closed orbit requires weaker correction strengths but they are still uncomfortably high. The same missing correctors with a missing monitor appears to improve the orbit correction and reduce the corrector strengths slightly. This means

that the situation is essentially unchanged, but, by removing the constraint at one monitor, the correction has been modified for the overall good at positions between the monitors. This can happen, since the correction routine acts on the sum of the squares at the monitors and although the excursions between the monitors tend to follow, it is not impossible that one increases while the other decreases. The conclusion of Table 9 is that the loss of a horizontal corrector (apart from the few that have near neighbours such as stations H5 and H6 and stations H8 and H9 of Figure 1) will have serious consequences for the operation.

Sensitivity to missing correctors		
	Uncorrected	**Corrected**
Horizontal corrector HC31 (upstream) removed		
Average of absolute maximum excursions [mm]	11.7	1.7
Maximum absolute excursion [mm]	26.2	3.1
Average of maximum corrector kicks [mrad]	-	0.93
Maximum corrector kick [mrad]	-	1.80
Horizontal corrector HC36 removed		
Average of absolute maximum excursions [mm]	11.7	2.7
Maximum absolute excursion [mm]	26.2	7.7
Average of maximum corrector kicks [mrad]	-	1.74
Maximum corrector kick [mrad]	-	5.64
Vertical corrector VC08 removed		
Average of absolute maximum excursions [mm]	4.1	0.9
Maximum absolute excursion [mm]	9.7	2.0
Average of maximum corrector kicks [mrad]	-	0.29
Maximum corrector kick [mrad]	-	0.57
Horiz. correctors HC31 (upstream)+HC36 removed		
Average of absolute maximum excursions [mm]	11.7	3.3
Maximum absolute excursion [mm]	26.2	11.1
Average of maximum corrector kicks [mrad]	-	1.10
Maximum corrector kick [mrad]	-	2.67
Vertical correctors VC08+VC33 removed		
Average of absolute maximum excursions [mm]	4.1	1.1
Maximum absolute excursion [mm]	9.7	2.1
Average of maximum corrector kicks [mrad]	-	0.29
Maximum corrector kick [mrad]	-	0.59
HC31 (upstream)+HC36 & monitor PX31 (upstream) removed		
Average of absolute maximum excursions [mm]	11.7	2.9
Maximum absolute excursion [mm]	26.2	9.1
Average of maximum corrector kicks [mrad]	-	1.03
Maximum corrector kick [mrad]	-	2.28
VC08+VC33& monitor PZ39 removed		
Average of absolute maximum excursions [mm]	4.1	1.6
Maximum absolute excursion [mm]	9.7	4.4
Average of maximum corrector kicks [mrad]	-	0.29
Maximum corrector kick [mrad]	-	0.60

Table 9 *Sensitivity to missing correctors at extraction (see Table 3 for comparison). Note that the values of Table 3 are obtained from the analysis of 1000 machine while this table refers to the analysis of 200 machines. This explains the lower values for the maximum absolute excursion and for the maximum corrector kick quoted above.*

The examples in Table 9 for the vertical plane are far less critical. The correctors are also more uniformly spaced in the vertical plane so that the examples given are very representative. Results in reasonable agreement with the ones shown in Table 9 have been obtained using the program AGILE with randomly-generated groups of 100 machines on the injection working point and for the same patterns of missing correctors and monitors.

2.9 Closed orbit degradation with time

Table 10 summarises the expectations for the growth of orbit distortion and corrector strengths after 2 and 5 years with 1000 randomly-generated (MAD) with non-space-charge conditions. It has been assumed [4] that on average the standard deviation of alignment errors will increase by:

$$\langle \Delta x + \delta e \rangle_{RMS}, \langle \Delta z + \delta e \rangle_{RMS}, \langle \Delta s + \delta e \rangle_{RMS} \quad \text{where } \delta e = 0.1 \text{ mm/yr}$$
$$\text{and } \langle \Delta\theta + \delta e \rangle_{RMS}, \text{ about any axis} \quad \text{where } \delta e = 0.1 \text{ mrad/yr.}$$

Natural growth of distortion and corrector strength with time

	Start	At 2 years	At 5 years
Alignment errors (standard deviation) [mm]	0.3	0.5	0.8
Tilt errors (standard deviation) [mrad]	0.3	0.5	0.8
Horizontal plane uncorrected			
Average of absolute maximum excursions [mm]	11.9	12.1	12.5
Maximum absolute excursion [mm]	37.7	37.3	36.9
Horizontal plane corrected			
Average of absolute maximum excursions [mm]	1.6	1.8	2.2
Maximum absolute excursion [mm]	3.5	3.8	4.4
Average of maximum corrector kicks [mrad]	0.94	1.02	1.21
Maximum corrector kick [mrad]	2.09	2.79	3.84
Vertical plane uncorrected			
Average of absolute maximum excursions [mm]	4.3	7.1	11.4
Maximum absolute excursion [mm]	13.4	22.4	36.1
Vertical plane corrected			
Average of absolute maximum excursions [mm]	0.63	1.04	1.66
Maximum absolute excursion [mm]	1.22	1.99	3.29
Average of maximum corrector kicks [mrad]	0.28	0.47	0.76
Maximum corrector kick [mrad]	0.65	1.09	1.75

Table 10 *Natural growth of distortion and corrector strength with time.*

Figures 12 (a) and (b) show the growth with time of orbit distortion before and after correction in the horizontal and vertical plane respectively. Figure 13 shows the behaviour of the corrector strength as a function of time.

It is evident from the data that the effect of misalignment is stronger in the vertical plane, where the distorted and corrected orbits and the corrector strength become almost three times larger after 5 years. Since the degradation with time will depend strongly on local conditions, Table 10 and Figures 12 and 13 can only be considered as a very general indication. However, the indication is that the corrected closed orbits in both planes will theoretically still be within tolerance after 5 years (i.e. $\pm$ 5 mm), but the required increases in corrector strength to achieve this will mean that in more

than 50% of the cases re-alignment will be necessary. Five-years between alignments appears to be a likely average.

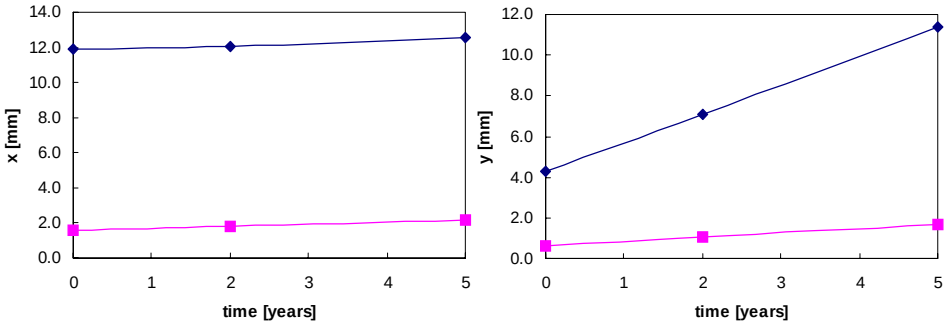

(a) Horizontal plane *(b) Vertical plane*

Figure 12 *Maximum average absolute excursion of the closed orbit before (rhombi) and after (squares) correction versus time.*

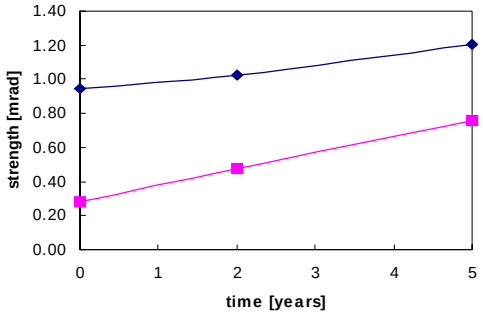

Figure 13 *Maximum average absolute horizontal (rhombi) and vertical (squares) corrector strength versus time*

3 CLOSED-ORBIT MANIPULATIONS

3.1 Closed-orbit control

The closed-orbit control at extraction will consist of two steps:

- Global correction to better than ± 5 mm in both planes. If this cannot be achieved, then the machine should be re-aligned.
- Addition of local corrections at sextupoles and septa. Although a local correction may degrade the orbit elsewhere, the overall distortion should not exceed ± 10 mm horizontally and ± 7.5 mm vertically.

The simplest form for a local correction is the application of closed bumps. Most local corrections will be made by pre-calculated 3- or 4-magnet bumps with an amplitude no bigger than 5 mm, as shown in Section 3.2 and 3.3. The bumps described in the next two sections represent a set of typical bumps able to correct the maximum residual orbit after global correction in some specific position. These simulations give the order of magnitude of the corrector strength for local manipulation and the possible shapes of the different local distortions even if they may not correspond to the exact and at present unpredictable needs of the real medical machine. In the horizontal plane, which is the more critical, it is also necessary to have a 5-magnet bump to control position and angle at the electrostatic septum and position at the magnetic septum, as shown in Section 3.4. In this case the desired bumps are found considering the angle error at the two septa after a global orbit correction.

3.2 3-magnet bumps

Sets of 3-magnet closed-orbit bumps have been prepared to control the beam excursion at specific positions of the ring. Table 11 lists the excitations and Figure 14 summarises the distribution and the form of the bumps for a machine on the extraction working point obtained with the program AGILE. The choice has been to create a 5 mm amplitude bump (see Section 2.1) at each beam monitor (for the monitor and corrector numbers, refer to Figure 1). When two correctors exist in the same drift space a choice has been made to minimise the total correction strength.

Excitations for 3-magnet bumps (see Figure 14)

Horizontal		Vertical	
Corrector or Monitor	**Kick [mrad] or Deflection [mm]**	**Corrector or Monitor**	**Kick [mrad] or Deflection [mm]**
HC MR 01	0.62	VC MR 03	0.48
PX MR 06	5	VC MR 08	-0.37
HC MR 06	-0.39	**PZ MR 09**	5
HC MR 11	0.62	VC MR 13	0.41
HC MR 06	0.60	VC MR 08	0.42
PX MR 11	5	VC MR 13	-0.35
HC MR 11	-0.001	**PZ MR 14**	5
HC MR 16	0.59	VC MR 18	0.46
HC MR 11	0.59	VC MR 13	0.45
PX MR 16	5	VC MR 18	-0.04
HC MR 16	-0.22	**PZ MR 19**	5
HC MR 21 (upstream)	0.55	VC MR 23	0.41
HC MR 16	0.56	VC MR 18	0.42
PX MR 21 (upstream)	5	VC MR 23	-0.04
HC MR 21 (upstream*)	-0.69	**PZ MR 24**	5
HC MR 26	0.47	VC MR 28	0.46
HC MR 21 (upstream*)	0.47	VC MR 23	0.47
PX MR 26	5	VC MR 28	-0.35
HC MR 26	-0.17	**PZ MR 29**	5
HC MR 31 (upstream)	0.61	VC MR 33	0.41
HC MR 26	0.60	VC MR 28	0.45
PX MR 31 (upstream)	5	VC MR 33	0.51
HC MR 31 (upstream*)	0.08	**PZ MR 34**	5
HC MR 36	0.61	VC MR 38	0.51
HC MR 31 (upstream*)	0.60	VC MR 33	0.45
PX MR 36	5	VC MR 38	0.04
HC MR 36	0.04	**PZ MR 39**	5
HC MR 01	0.45	VC MR 03	0.41
HC MR 36-3	0.46	VC MR 38	0.42
PX MR 01-7	5	VC MR 03	-0.06
HC MR 01-8	-0.76	**PZ MR 04**	5
HC MR 06-2	0.62	VC MR 08	0.49

* When two correctors exist in the same drift space a choice has been made to minimise the total correction strength.

Table 11 *Excitations for 3-magnet bumps [on extraction working point: $Q_x = 1.667$, $Q_z = 1.720$].*

It is clear from Table 11 and Figure 14 that the 3-magnet bumps are well-behaved in both horizontal and vertical plane.

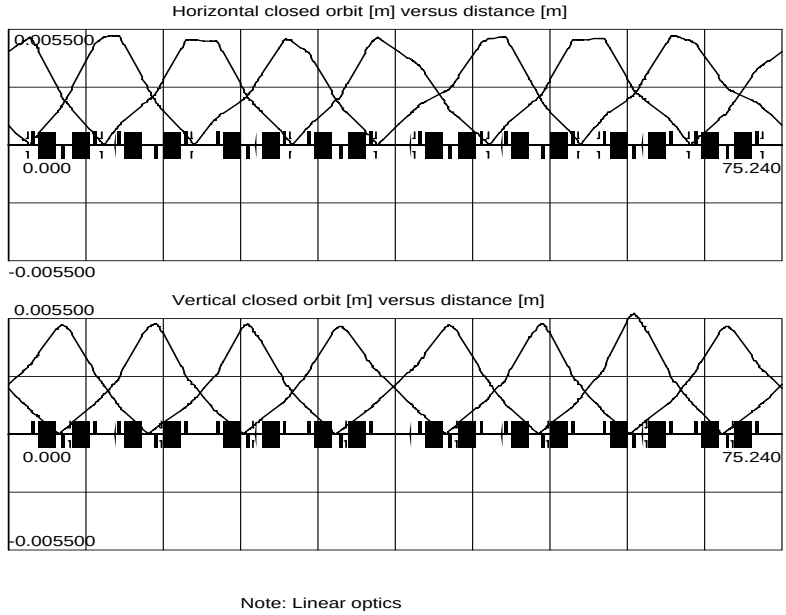

Figure 14 3-magnet bumps set to 5 mm at an intermediate beam monitor.

4-magnet bumps

Sets of 4-magnet closed-orbit bumps have been prepared to control the beam excursion and angle at specific positions of the ring. Table 12 lists the excitations and Figure 15 summarises the distribution and the form of the bumps for a machine on the extraction working obtained with the program AGILE. The choice has been to create a 5 mm amplitude bump with 0 mrad slope at the appropriate beam monitor (for the monitor and corrector names, refer to Figure 1). When two correctors exist in the same drift space a choice has been made to minimise the total correction strength.

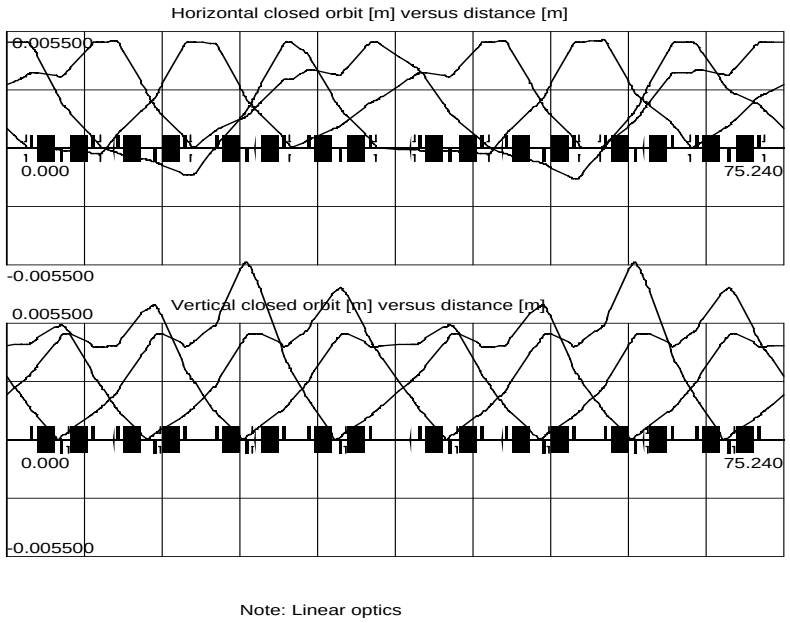

Figure 15 *4-magnet bumps set to 5 mm, 0 mrad at an intermediate monitor.*

Excitations for 4-magnet bumps (see Figure 15)			
Horizontal		**Vertical**	
Corrector or Monitor	**Kick [mrad] or Deflection [mm]**	**Corrector or Monitor**	**Kick [mrad] or Deflection [mm]**
HC MR 01	-0.03	VC MR 03	0.41
HC MR 06	0.62	VC MR 08	0.36
PX MR 11	5	**PZ MR 09**	5
HC MR 11	-0.03	VC MR 13	-0.21
HC MR 16	0.59	VC MR 18	0.74
HC MR 06	-0.15	VC MR 08	-0.38
HC MR 11	0.59	VC MR 13	0.31
PX MR 16	5	**PZ MR 14**	5
HC MR 16	-0.37	VC MR 18	-0.36
HC MR 21 (upstream)	0.55	VC MR 23	0.57
HC MR 11	0.38	VC MR 13	0.42
HC MR 16	0.41	VC MR 18	0.40
PX MR 21 (upstream)	5	**PZ MR 19**	5
HC MR 21 (upstream)	-0.32	VC MR 23	0.33
HC MR 26	0.46	VC MR 28	0.48
HC MR 16	0.30	VC MR 18	0.38
HC MR 21 (upstream)	0.12	VC MR 23	0.53
PX MR 26	5	**PZ MR 24**	5
HC MR 26	0.04	VC MR 28	-0.01
HC MR 31 (upstream)	0.60	VC MR 33	0.50
HC MR 21 (upstream)	-0.02	VC MR 23	0.42
HC MR 26	0.61	VC MR 28	0.34
PX MR 31 (upstream)	5	**PZ MR 29**	5
HC MR 31 (upstream)	0.05	VC MR 33	-0.21
HC MR 36	0.61	VC MR 38	0.74
HC MR 26	-0.02	VC MR 28	0.37
HC MR 31 (upstream)	0.60	VC MR33	0.30
PX MR 36	5	**PZ MR 34**	5
HC MR 36	0.20	VC MR 38	0.36
HC MR 01	0.45	VC MR 03	0.57
HC MR 31 (downstream)	0.43	VC MR 33	0.42
HC MR 36	0.32	VC MR 38	0.40
PX MR 01	5	**PZ MR 39**	5
HC MR 01	-0.42	VC MR 03	0.32
HC MR 06	0.61	VC MR 08	0.51
HC MR 36	0.31	VC MR 38	0.38
HC MR 01	0.09	VC MR 03	0.53
PX MR 06	5	**PZ MR 04**	5
HC MR 06	0.04	VC MR 08	-0.01
HC MR 11	0.60	VC MR 13	0.50

* When two correctors or monitors exist in the same drift space a choice has been made to minimise the total correction strength.

Table 12 *Excitations for 4-magnet bumps [Q_x = 1.667, Q_z = 1.720].*

The 4-magnet bumps are well-behaved in the horizontal plane, while in the vertical have large peaks that go beyond the excursion at the monitor; these bumps are less useful.

3.4 5-magnet bump

The distance from the stable fixed point to the electrostatic septum determines the spiral step and the geometry of the extraction. In order to maintain constant optics in the extraction transfer lines, the horizontal closed orbit must be controlled at the electrostatic and magnetic septa. Ideally, two 4-magnet bumps that control the

position and angle at both septa are needed. Unfortunately, there is space for only one horizontal corrector between the electrostatic and magnetic septa. This means that the 4-magnet bumps that would normally be used overlap such that corrections at one septum would affect the other. This has been overcome by designing a 5-magnet bump that controls position and angle at the electrostatic septum with 2 correctors upstream of the electrostatic septum (see Figure 16) and position at the magnetic septum with the single corrector between the two septa. The magnetic septum must then adjust the angle of the extracted beam. For the circulating beam two correctors in the next straight sections close the bump.

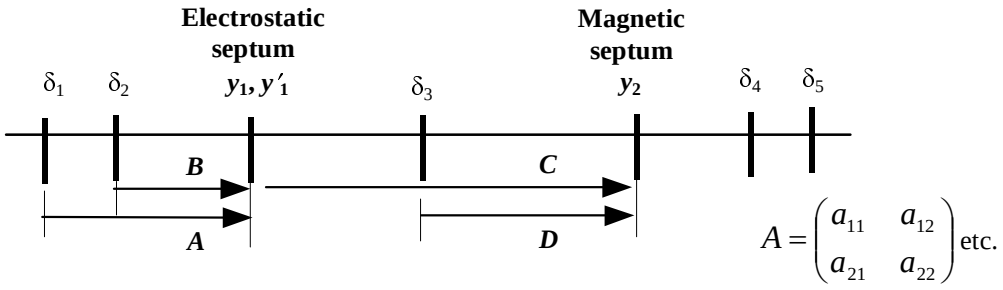

Figure 16 *Layout of the 5-magnet bump for extraction.*

In the PIMMS machine, there are a number of local considerations:

- Since the phase shift between the electrostatic and magnetic septa is only 51°, it would require an exceptional field error to cause the maximum orbit excursion (from Table 3, maximum horizontal excursion after correction = 3.5 mm) to occur with opposite signs at the two septa. It is much more likely that the two excursions will have the same sign or be within the much smaller range (± 1.5 mm).

- There are no sextupoles between the two septa. This means that the gap opened by the electrostatic septum between the circulating separatrix and the extracted segment should be independent of the orbit distortion and the bump height.

- There are two chromaticity sextupoles in the entry section of the bump. The first is just after the first correction where the amplitudes are quasi-zero, but the other may 'see' large amplitudes. Under extreme conditions, it may therefore be necessary to steer the bump slightly to account for the influence of this lens.

The first two correctors are set according to,

$$\begin{pmatrix} \delta_1 \\ \delta_2 \end{pmatrix} = \begin{pmatrix} b_{22} & -b_{12} \\ -a_{22} & a_{12} \end{pmatrix} \begin{pmatrix} y_1 \\ y_1' \end{pmatrix} \tag{10}$$

and the third corrector is set according to

$$\delta_3 = \frac{y_2 - c_{11} y_1 - c_{12} y_1'}{d_{12}} . \tag{11}$$

The angle at the magnetic septum will then be

$$y_2' = c_{21} y_1 + c_{22} y_1' + d_{22}\left(\frac{y_2 - c_{11} y_1 - c_{12} y_1'}{d_{12}}\right). \qquad (12)$$

Finally, the bump is closed by δ_4 and δ_5 in the same way as it is excited by δ_1 and δ_2.

The distributions of the angle errors (absolute values) at the two septa after a global obit correction have been calculated (see Figures 17 and 18) for 1000 machines on the extraction working point. Table 13 summarises the main parameters obtained from the analysis of the simulations. The expected position errors are assumed to have the same characteristics as the closed-orbit distortion after correction (from Table 3, 3.5 mm). Based on these numbers, the 5-magnet bump will be designed to cover ± 3.5 mm at the electrostatic and magnetic septa and ± 0.25 mrad at the electrostatic septum (75% of the orbits). The magnetic septum will then have a residual angle to correct of less than ± 0.20 mrad.

Angular distributions at the electrostatic and magnetic septa after global orbit correction

	Electrostatic septum	**Magnetic septum**
Maximum angle error [mrad]	1.15	0.93
Average angle error [mrad]	0.15	0.12
Angle for 75% of the distribution [mrad]	0.25	0.20

Table 13 *Angular distributions (absolute value) at the electrostatic and magnetic septa after global orbit correction.*

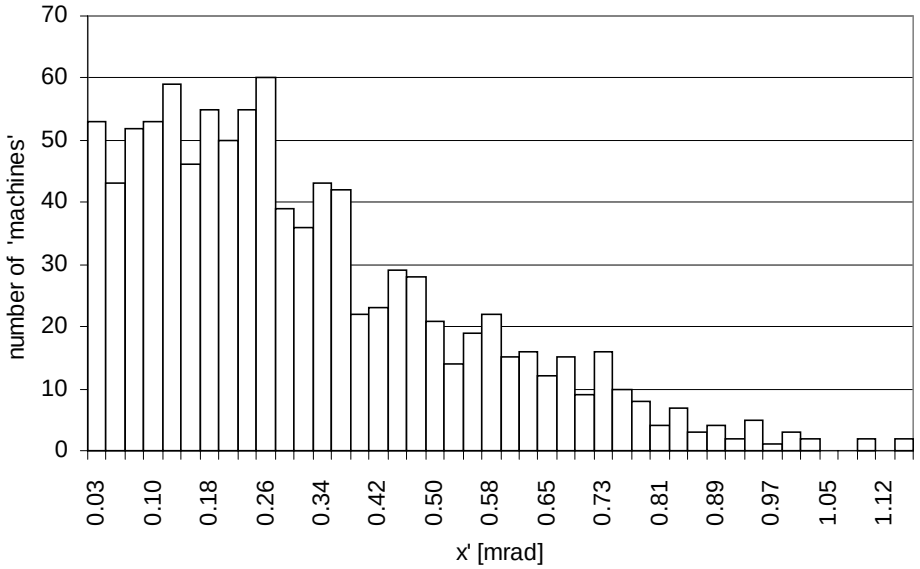

Figure 17 *Expected distribution of the angle error (absolute value) at the electrostatic septum after a global closed-orbit correction (Q_x = 1.667, Q_z = 1.720).*

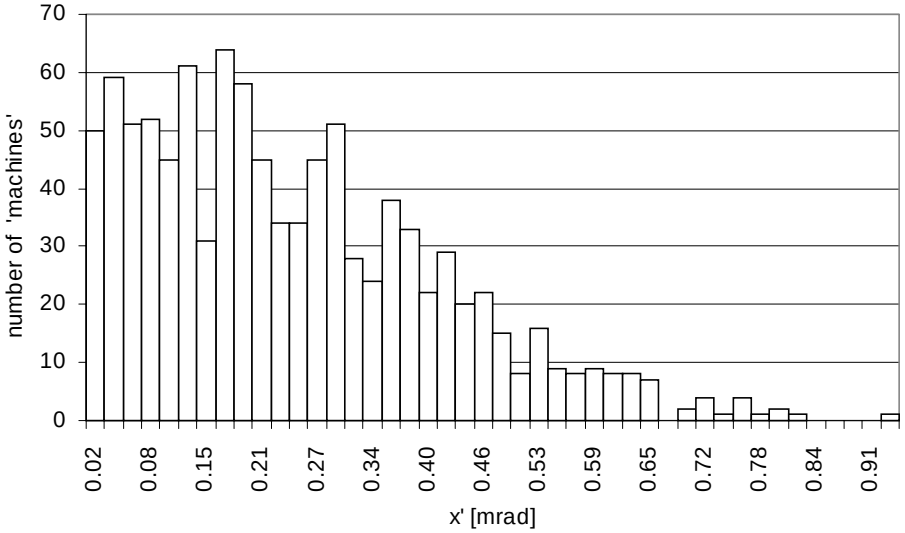

Figure 18 *Expected distribution of the angle error (absolute value) at the magnetic septum after a global closed-orbit correction (Q_x = 1.667, Q_z = 1.720).*

Figure 19 shows some limiting cases for the 5-magnet bump and Table 14 lists the corresponding kick strengths.

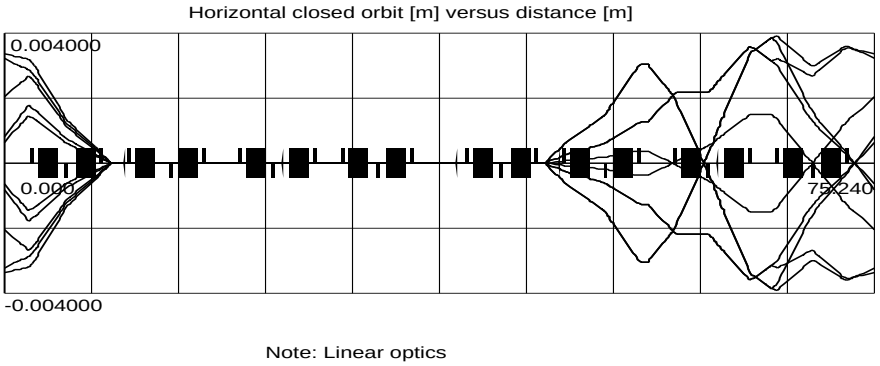

Figure 19 *Some examples of the 5-magnet extraction bump [Q_x = 1.667, Q_z = 1.720].*

Some examples of the 5-magnet extraction bump

Electrostatic septum		**Magnetic septum**	**δ1 HC 26**	**δ2 HC 31***	**δ3 HC 36**	**δ4 HC 01**	**δ5 HC 06**
3.5 mm	-0.25 mrad	3.5 mm	0.150 mrad	0.403 mrad	0.416 mrad	-0.192 mrad	0.387 mrad
3.5 mm	0.25 mrad	3.5 mm	-0.363 mrad	0.423 mrad	-0.142 mrad	-0.079 mrad	0.348 mrad
3.5 mm	-0.25 mrad	0.0 mm	0.150 mrad	0.403 mrad	-0.004 mrad	0.499 mrad	-0.174 mrad
3.5 mm	0.25 mrad	0.0 mm	-0.363 mrad	0.423 mrad	-0.562 mrad	0.612 mrad	-0.214 mrad
1.5 mm	0.0 mrad	-1.5 mm	-0.046 mrad	0.117 mrad	-0.302 mrad	0.534 mrad	-0.324 mrad

* Upstream HC-31

Table 14 *Some examples of the 5-magnet extraction bump.*

4 SPECIFICATIONS FOR CORRECTORS

The correctors must be able to meet the demands of both the global orbit correction and the local corrections at top energy. The evaluation must be made on the extraction working point, where the magnetic rigidity is largest. Table 15 summarises the analysis of the horizontal and vertical corrector strength on the extraction working point (see also Figures 6 and 7, Section 2.5).

Prognosis for closed orbits at extraction and their correction		
	Horizontal	**Vertical**
Average of max. corrector kicks [mrad]	0.94	0.28
Max. corrector kick [mrad]	2.09	0.65
% of orbits corrected with kicks up to the average value	77%	75%
Kick necessary to correct 95% of the orbits [mrad]	1.30	0.39

Table 15 *Prognosis for closed orbits at extraction and their correction.*

Table 15 shows that correctors with a strength of 0.94 mrad kicks in the horizontal plane will correct 77% of the orbits and 0.28 mrad 75% in the vertical plane. A similar philosophy can be applied to the local bumps i.e. a maximum kick strength is chosen that will satisfy the maximum specified amplitude in more than 75% of the cases. Inspection of Table 11 (3-magnet bumps), Table 12 (4-magnet bumps) and Table 14 (5-magnet bump) indicates that 0.58 mrad is sufficient to fulfil this criterion in the horizontal plane and 0.47 in the vertical plane. In the few cases that are not covered, the maximum kick is typically 0.75 mrad. Summing these requirements linearly, implies strengths of 1.52 mrad in the horizontal plane and 0.75 mrad in the vertical plane. Table 3 also shows that there is some margin between the allowable closed-orbit tolerances in the two planes and the prognostics for the correction. This margin should make the above estimates rather safe and also help to absorb errors from missing monitors and/or correctors and degradation of the alignment with time. At the same time, it is best to limit the maximum corrector strengths as far as possible, since excessive strength will only contribute to imprecision when running the lower-rigidity proton beams. The proposal is therefore to build correctors with:

Proposed horizontal maximum corrector strength = 1.5 mrad
Proposed vertical maximum corrector strength = 0.75 mrad.

The lower value in the vertical plane fortuitously compensates for the need for a larger aperture.

The horizontal correction dipole field for maximum kick in a 0.2 m magnetic length unit ranges from $B = 0.0045$ T for injection of protons at 20 MeV ($B = 0.0026$ T at 7 MeV) to $B = 0.0008$ T for the first extraction flat-top for protons and $B = 0.045$ T for the last flat-top for carbon ions. As the required orbit precision is stricter at extraction ($\pm$ 0.1 mm versus $\pm$ 1 mm at injection [7]) and the chosen maximum corrector strength corresponds to a beam maximum excursion of about $\pm$ 10 mm, an 11-bit DAC converter will be necessary for the required precision.

5 CONCLUSIONS

The results of the simulations indicate that the closed-orbit margin specified for PIMMS is more comfortable in the vertical plane than in the horizontal. Simulations of a freshly-aligned machine with non-space-charge conditions show that 41% of the machines in the horizontal plane and 96% in the vertical plane are within the allowed closed-orbit margin before correction. After correction, all machines would also be well within the stricter tolerances for extraction.

The situation becomes more critical at the injection energy for the highest intensity proton beam due to space-charge forces and dipole remanent field errors. At 20 MeV 30% of the machines in the horizontal plane and 70% in the vertical plane would be within the allowed closed-orbit margins and could be injected with full intensity without beam loss. Simulations with injection energies lower than 20 MeV show a non-negligible deterioration of the orbits. Consequently, fewer orbits before correction are within the global margins; at 7 MeV these figures drop to 12% horizontally and 24% vertically. However, after correction, all machines are within tolerance and would also be within the stricter tolerances for extraction. Technically the vertical size of the proton beam is just outside the nominal limit at 7 MeV and this would also make injection more difficult initially.

Simulations with missing position monitors and correction dipoles show that any reduction in the number of monitors and correctors leads to a serious deterioration of the orbit. The situation is more critical in the horizontal plane when consecutive monitors or correctors without a nearby neighbour fail. It has been shown that removing a uniformly-spaced corrector approximately doubles the amplitude of the corrected closed orbits and the corrector strength. Removing more than one corrector per plane leads to a deterioration of the orbit to the point where the tail of the distribution after correction is outside tolerance. Therefore the correction and monitoring system shown in Figure 1 should be regarded as the minimum set of elements necessary for a good correction scheme.

Simulations of orbit degradation with time due to misalignment of the magnetic elements and position monitors are mainly qualitative because the degradation depends strongly on local conditions. It is evident from the data that the effect of misalignment is stronger in the vertical plane, where the distorted and corrected orbits and the corrector strengths become almost three times larger 5 years after alignment. Due to the required increase in corrector strength a five-year period between alignments appears to be a likely average.

The simulation of local orbit errors during extraction shows that with the planned position monitor and corrector layout it is possible to have a good local orbit control at critical positions using 3- and 4-magnet closed bumps in both horizontal and vertical plane. In the horizontal plane a 5-magnet bump controls the position and angle at the electrostatic septum and position at the magnetic septum.

The maximum corrector strengths (1.5 mrad for the horizontal correction dipoles and 0.75 mrad for the vertical correction dipoles) were defined on the requirements of the global closed-orbit correction and local bumps. A compromise was made between adding a safety margin for element failure and misalignment with time and the

advantage of limiting the corrector strength to reduce the ripple ‘seen’ by the lowest rigidity beams.

The possibility of lowering the injection energy of the proton beam, preferably to 7 MeV in order to use a single linac for both particle species, has been shown to be feasible. However, the situation becomes more critical as the injection energy is lowered in terms of both deterioration of the closed orbit and increase of the beam size. It was shown that the machine is very susceptible to the loss of position monitors and correctors at all energies. Even if it is difficult to give an overall quantitative evaluation, the concern is that the combined operational problems, already critical at 20 MeV, may prove at 7 MeV to be inconsistent with the level of reliability needed in a hospital environment.

ACKNOWLEDGEMENTS

This work was performed at CERN, within the framework of the Proton-Ion Medical Machine Study. I would like to thank Jacques Bosser, Phil Bryant (PS Division) and Marco Pullia (Fondazione TERA) for many useful discussions.

REFERENCES

[1] E. D. Courant and H. S. Snyder, *Theory of the alternating gradient synchrotron*, Annals of Physics n^0 3 (1958), 1-48.

[2] P. J. Bryant, AGILE program for synchrotron lattice design, http://nicewww.cern.ch/ ~bryant.

[3] H. Grote, F. Iselin *The MAD program, Users’ Reference Manual*, CERN/SL/90-13 (AP), (1990).

[4] B. Autin and Y. Marti, *Closed Orbit Correction of A. G. machines using a limited number of magnets*, CERN ISR-MA/73-17 (1973).

[5] M. Mayoud, Leader of the CERN Survey Group, Private Communication (1996).

[6] P. J. Bryant, *PIMMS Field Quality, Field Setting and Mechanical Tolerances*, Teach-in number 3, CERN (1996).

[7] L. Badano, *Beam diagnostics and monitors for the PIMMS Synchrotron*, CERN/PS 99-037 (DI) (1999).

[8] K. D. Gross, M. Pavlovic ed., *Proposal for a Dedicated Ion Beam Facility for Cancer Therapy*, RHU, DKFZ, GSI, FZR (1998).

[9] M. Crescenti, *Beam Optics of PIMMS Injection Lines*, to be published as CERN Divisional Report.

[10] L. Badano, M. Benedikt, P. Bryant, M. Crescenti, P. Holy, P. Knaus, A. Maier, M. Pullia, S. Rossi, *Proton-Ion Medical Machine Study (PIMMS) – Part II*, to be published as CERN Divisional Report.